Monthly Notices
of the
ROYAL ASTRONOMICAL SOCIETY

Mon. Not. R. Astron. Soc. **407,** 1728–1738 (2010) doi:10.1111/j.1365-2966.2010.17000.x

Characterization of 15 overlooked Ruprecht clusters with ages within 400 Myr and 3 Gyr

C. Bonatto★ and E. Bica

Departamento de Astronomia, Universidade Federal do Rio Grande do Sul, Av. Bento Gonçalves 9500 Porto Alegre 91501-970, RS, Brazil

Accepted 2010 May 11. Received 2010 May 10; in original form 2010 April 20

ABSTRACT

We derive fundamental, structural and photometric parameters of 15 overlooked Ruprecht (hereafter Ru) star clusters by means of Two-Micron All-Sky Survey photometry and field-star decontamination. Ru 1, 10, 23, 26, 27, 34, 35, 37, 41, 54, 60, 63, 66 and 152 are located in the third Galactic quadrant, while Ru 174 is in the first. With the constraints imposed by the field-decontaminated colour–magnitude diagrams and stellar radial density profiles (RDPs), we derive ages in the range 400 Myr – 1 Gyr, except for the older Ru 37, with ∼3 Gyr. Distances from the Sun are within $1.5 \lesssim d_{\odot}(\mathrm{kpc}) \lesssim 8.0$. The RDPs are well-defined and can be described by a King-like profile for most of the radial range, except for Ru 23, 27, 41, 63 and 174, which present a conspicuous stellar density excess in the central region. The clusters dwell between (or close to) the Perseus and Sagittarius-Carina arms. We derive evidence in favour of cluster size increasing with distance to the Galactic plane (Z_{GP}), which is consistent with a low frequency of tidal stress associated with high-$|Z_{\mathrm{GP}}|$ regions. The clusters are rather faint even in the near-infrared, with apparent integrated J magnitudes within $6.4 \lesssim m_J \lesssim 9.8$, while their absolute magnitudes are $-6.6 \lesssim M_J \lesssim -2.6$. Extrapolation of the relation between M_V and M_J, derived for globular clusters, suggests that they are low-luminosity optical clusters, with $-5 \lesssim M_V \lesssim -1$.

Key words: open clusters and associations: general – Galaxy: structure.

1 INTRODUCTION

In general, open clusters (OCs) are formed and evolve in – or close to – the Galactic disc. As a consequence of their orbits, they are constantly suffering tidal stress from Galactic substructures and undergoing different degrees of mass loss that, in most cases, might lead to cluster dissolution. Indeed, the vast majority of the OCs do not survive even the embedded phase (e.g. Lada & Lada 2003), and few reach ages older than $\sim 10^8$ yr (e.g. Goodwin & Bastian 2006).

As systems in which the balance between velocity dispersion and escape velocity plays a vital role, OC stellar distributions change continually as a function of time because of mass segregation and evaporation, tidal interactions with the disc and/or bulge, encounters with giant molecular clouds, as well as mass loss associated with stellar evolution. On average, these processes tend to accelerate the cluster dynamical evolution and change the internal structure in varying degrees. Indeed, near the solar circle, theoretical and observational evidence (e.g. Oort 1958; Spitzer 1958; Baumgardt & Makino 2003; Goodwin & Bastian 2006; Lamers & Gieles 2006; Khalisi, Amaro-Seoane & Spurzem 2007; Piskunov et al. 2007) suggest a mass-dependent disruption time-scale of a few 10^8 yr. As a consequence, most OCs end up completely dissolved in the Galactic stellar field (e.g. Lamers et al. 2005) or leave only poorly populated remnants (Pavani & Bica 2007 and references therein), long before reaching ∼1 Gyr of age.

Reflecting the above age/dissolution effect, only ≈13 per cent of the ≈1100 OCs with known age listed in WEBDA[1] are older than 1 Gyr, while ≈45 per cent have an age between 100 Myr and 1 Gyr, and ≈42 per cent are younger than 100 Myr. So, besides the obvious importance of deriving reliable astrophysical parameters for as yet unstudied clusters, the unambiguous characterization of OCs older than several 10^8 yr will increase the statistics of objects undergoing the dissolution phase. This, in turn, can be used for better determining the time-scale for cluster dissolution in the Galaxy.

Cluster data bases such as WEBDA still contain many unstudied objects that, over the years, have been identified as star cluster candidates, usually based on the appearance in optical images. Not surprisingly, close investigations of some of these overlooked objects have uncovered a number of actual OCs (e.g. Carraro, Janes & Eastman 2005; Carraro et al. 2006a; Carraro, Subramaniam & Janes 2006b). Besides, since young OCs are relatively easy to identify (because of the presence of bright stars) even at relatively large

★E-mail: charles@if.ufrgs.br

[1] www.univie.ac.at/webda

© 2010 The Authors. Journal compilation © 2010 RAS

Downloaded from http://mnras.oxfordjournals.org/ at FundaÃ§Ã£o Coordenação de Aperfeiçoamento de Pessoal de NÃ-vel Superior on February 24, 2014

distances, the overlooked clusters, in general, are as old as several 10^8 yr, sometimes reaching a few Gyr (e.g. the ∼4 Gyr old OC Berkeley 56; Carraro et al. 2006b).

Based on the optical *Catalogue of Star Clusters and Associations* of Alter et al. (1970), WEBDA lists the coordinates of 171 OC candidates originally found by J. Ruprecht (classified as Ruprecht clusters, hereafter Ru). However, only 79 have been so far confirmed as OCs, having determinations of fundamental parameters, such as the age, reddening and distance from the Sun. In this paper we derive fundamental and structural parameters for 15 of these overlooked Ruprecht OCs, 12 of these not previously studied, and the remaining 3 with inconsistent determinations (Sections 4 and 5). Steps taken in this work can be summarized as follows: (i) Two-Micron All-Sky Survey (2MASS)[2] photometry is extracted in a wide circular region centred on a given cluster; (ii) we apply field-star decontamination to uncover the intrinsic colour–magnitude diagram (CMD) morphology, which is essential for a proper derivation of reddening, age and distance from the Sun; and (iii) we apply colour–magnitude filters to produce more contrasted stellar radial density profiles (RDPs). In particular, field-star decontaminated CMDs constrain the fundamental parameters more than the raw (observed) photometry, especially for low-latitude and/or bulge-projected OCs (e.g. Bica, Bonatto & Camargo 2008, and references therein).

This paper is organized as follows. In Section 2, we present optical images of the sample objects. In Section 3, we discuss the 2MASS photometry and build the field-star decontaminated CMDs. In Section 4, we derive fundamental cluster parameters. In Section 5, we derive structural parameters. In Section 6, we investigate relations among parameters and with respect to their location in the Galaxy. Concluding remarks are given in Section 7.

2 THE SAMPLE OF OVERLOOKED RUPRECHT CLUSTERS

We started by examining the optical images of the objects in order to identify the best candidates to be further studied with 2MASS photometry (Section 3). In short, the selection criteria were (i) a relatively conspicuous stellar density excess (typical of a star cluster), (ii) a foreground/background not excessively dense and (iii) an angular size larger than ∼1 arcmin (a smaller size might indicate an excessively distant object, too faint to be detected with 2MASS). The goal was to focus on objects that would result in reliable determinations of fundamental (Section 4) and structural (Section 5) parameters. The above search resulted in 12 unstudied OCs. Besides these, we also included three other cases somewhat studied, but with inconsistent parameters (Sections 4 and 5).

The sample of Ruprecht clusters that came up from the above search is shown in 5×5 arcmin^2 B images (Figs 1 and 2), taken from Leicester Database and Archive Service (LEDAS).[3] Note that the images are centred on different coordinates (Table 1) than those given in WEBDA. By default, we start the 2MASS analyses by assuming the WEBDA coordinates as cluster centre. However, in most cases the RDPs built after field decontamination – to maximize membership probability (Section 5), presented a dip in the innermost radial bin. So, the central coordinates were computed again to match the absolute maximum in the stellar surface density (e.g. Fig. 3). In most cases, the difference between the original and recomputed central coordinates is slight, of the order of 1 arcmin, thus well within the estimated optical diameter (Column 7 of Table 1).

The images match our selection criteria in different degrees. For instance, the highest compactness levels occur with Ru 35, 37, 41, 54, 60, 63 and 152. Ru 1, 10, 23 and 27 are projected on the least contaminated fields, with Ru 174 in the densest. Note that the bright (foreground) star 6 Pup (K 3 III) is located at ≈2 arcmin to the north-west of the central coordinates of Ru 37.

3 PHOTOMETRIC ANALYSIS

Photometry for the sample clusters was extracted from VizieR[4] in a circular field of radius $R_{\rm ext}$ =60 arcmin. Such a wide extraction area provides the required statistics for the determination of the background level (Section 5) and the colour–magnitude characterization of the field stars (see below). To preserve the photometric quality and, at the same time, work with a statistically significant number of stars, only stars with J, H and $K_{\rm s}$ errors lower than 0.15 mag were used. Reddening corrections are based on the absorption relations $A_J/A_V = 0.276$, $A_H/A_V = 0.176$, $A_{K_S}/A_V = 0.118$ and $A_J = 2.76 \times E(J-H)$ given by Dutra, Santiago & Bica (2002), with $R_V = 3.1$, considering the extinction curve of Cardelli, Clayton & Mathis (1989).

Except for Ru 174 (at $\ell \approx 78^\circ$, near the border between the first and second quadrants), the remaining clusters belong to the third Galactic quadrant (Table 1), which would make field-star contamination a minor issue (e.g. Bica et al. 2008). However, given the relatively poorly populated nature of the present sample (Figs 1 and 2), it is important to take the field-star contamination into account to derive more constrained parameters. In particular, we wish to work with CMDs in which cluster evolutionary sequences and field stars are disentangled.

For this purpose, we work with a statistical decontamination algorithm that has been developed by our group for the proper identification and characterization of star clusters, especially those near the Galactic equator and/or with important fractions of faint stars. The algorithm is applied to the 2MASS photometry, which can provide the spatial and photometric uniformity required for wide extractions and high star-count statistics.

Working with the wide circular extractions, we start by defining the cluster and comparison field regions.[5] CMDs extracted from the cluster region for our objects are shown in Figs 3–5 (top panels). These can be contrasted with the representative (i.e. equal-area) comparison field CMDs (middle panels). It is important to note that the equal-area field extraction is used only for qualitative comparisons, since the algorithm uses the wide surrounding area (as defined above) for more statistical representativeness. Our approach implicitly assumes that the field colour–magnitude distribution (i) is statistically representative of the cluster contaminants and (ii) is rather spatially uniform. These assumptions are somewhat matched in the third Galactic quadrant. A detailed description of the decontamination algorithm can be found in Bonatto & Bica (2007b) and

[2] The 2MASS, All Sky data release (Skrutskie et al. 1997) – http://www.ipac.caltech.edu/2mass/releases/allsky/

[3] LEDAS Digitized Sky Survey (DSS)/DSS-II service on ALBION; http://ledas-www.star.le.ac.uk/DSSimage

[4] http://vizier.u-strasbg.fr/viz-bin/VizieR?-source=II/246

[5] This step is iterative, since we first have to build the RDP (Section 5) to estimate the cluster size and the location of the comparison field. After applying the algorithm, we build the colour–magnitude filters for the decontaminated cluster CMD. Then we re-build the RDP, re-compute the cluster size and run again the decontamination algorithm.

Downloaded from http://mnras.oxfordjournals.org/ at FundaÃ§Ã£o CoordenaÃ§Ã£o de AperfeiÃ§oamento de Pessoal de NÃvel Superior on February 24, 2014

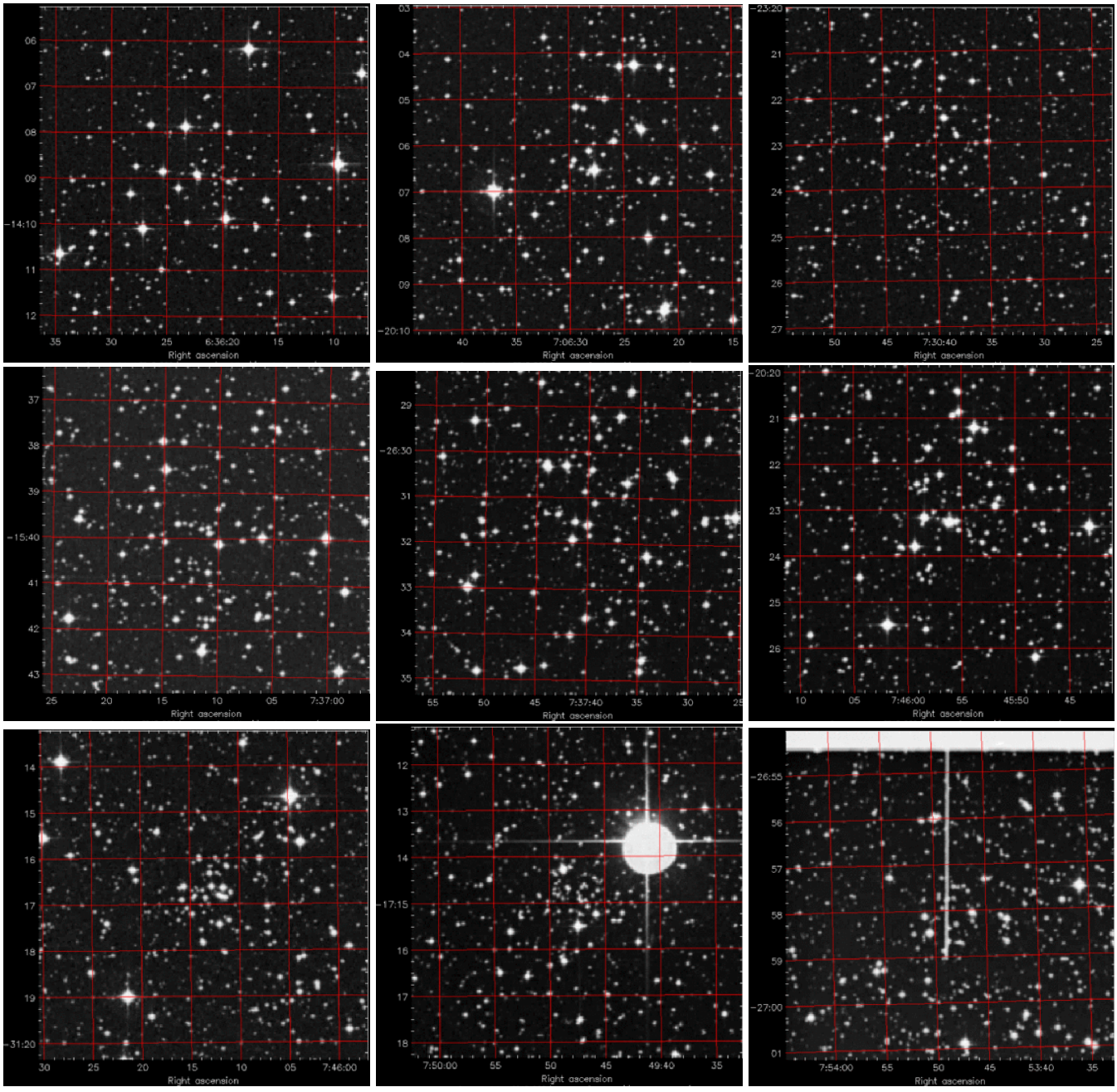

Figure 1. All panels display 5 × 5 arcmin^2 DSS-I B images. From left to right: Ru 1, 10 and 23 (top); Ru 26, 27 and 34 (middle); Ru 35, 37 (with the bright K 3 III star 6 Pup at ≈2 arcmin to the north-west) and Ru 41 (bottom). Plate flaws show up in the image of Ru 41. Orientation: north at the top and east at left.

Bonatto & Bica (2010). For clarity, we provide below only a sketch on how it works.

The cluster CMD is divided into a 3D grid of cells with axes along the J magnitude and the $(J-H)$ and $(J-K_s)$ colours. Then, we compute the probability of a given star to be found in a particular cell [i.e. for a star with measured magnitude and colour uncertainties $J \pm \sigma_J$, $(J-H) \pm \sigma_{(J-H)}$ and $(J-K_s) \pm \sigma_{(J-K_S)}$, the probability is proportional to the difference between the error function computed at the J, $(J-H)$ and $(J-K_s)$ borders of the cell]. This step is done for all stars and cells, resulting in a number density of member + field stars for each cell (η_{tot}). The same steps are applied to the comparison field CMD, from which we estimate the field number density (η_{fs}) for each cell. Next, for each cluster cell we subtract the corresponding field number density to obtain a decontaminated number density ($\eta_{mem} = \eta_{tot} - \eta_{fs}$). Finally, η_{fs} is converted back into number of stars and subtracted from each cell, and the N^{cell}_{clean} stars that remain in the cell are identified. We also compute the subtraction efficiency (f_{sub}), which is the sum over all cells of the difference between the expected number of field stars (which usually is fractional) and the number of stars effectively subtracted (integer). In all cases, we obtained $f_{sub} > 90$ per cent.

The above procedure is repeated for 729 different setups (allowing for variations on cell size and grid positioning). Each setup produces a total number of member stars $N_{mem} = \sum_{cell} N^{cell}_{clean}$, from which we compute the expected total number of member stars $\langle N_{mem} \rangle$ by averaging out N_{mem} over all setups. Stars (identified

Downloaded from http://mnras.oxfordjournals.org/ at FundaÃ§Ã£o CoordenaÃ§Ã£o de AperfeiÃ§oamento de Pessoal de NÃvel Superior on February 24, 2014

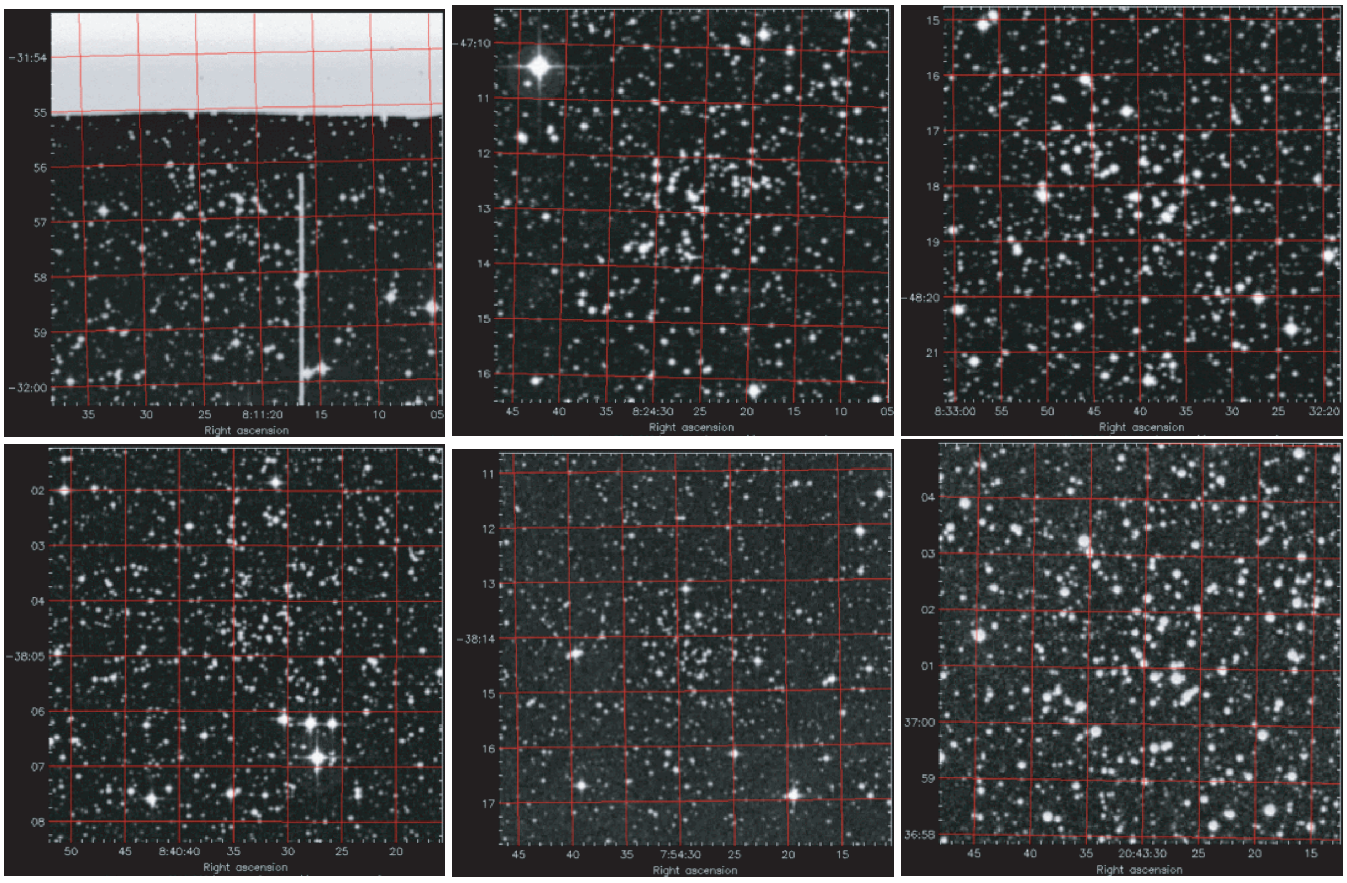

Figure 2. Same as Fig. 1 for the remaining clusters. From left to right: Ru 54, 60 and 63 (top); Ru 66, 152 and 174 (bottom). Plate flaws show up in the image of Ru 54.

above) are ranked according to the number of times they survive all runs, and only the $\langle N_{\rm mem}\rangle$ highest ranked stars are considered cluster members and transposed to the respective decontaminated CMD. The decontaminated $J \times (J - H)$ CMDs of the present sample are shown in Figs 3–5 (bottom panels).

Our decontamination approach relies upon differences in the stellar surface density measured in CMD cells of separate (cluster and comparison field) spatial regions. For a star cluster, which can be characterized by a single-stellar population projected against a (rather uniform) Galactic stellar field, the decontaminated surface density is expected to present a marked excess at the assumed cluster position. We illustrate this point by means of the stellar surface density (σ, in units of stars arcmin^{-2}) of Ru 1 (Fig. 6), before (top-left panel) and after (top-right panel) decontamination. The respective isopleths are also shown (bottom), in which cluster size and geometry can be appreciated. Clearly, the decontamination largely enhanced the cluster/background contrast, revealing a marked central excess in the surface density distribution, together with a well-defined, approximately round and narrow stellar distribution.

4 DERIVATION OF FUNDAMENTAL PARAMETERS

The presence of somewhat distant and evolved (in different degrees) OCs is suggested by the $J \times (J - H)$ CMDs built with the raw photometry of the sample clusters (top panels of Figs 3–5). This is clearly confirmed in the decontaminated CMDs (bottom panels), in which conspicuous giant clumps and red giant branches can be seen in some cases (e.g. Ru 10, 23, 60 and 66).

We derive the fundamental (reddening, age and distance from the Sun) parameters by means of the decontaminated CMD morphologies together with Padova isochrones (Girardi et al. 2002) computed with the 2MASS J, H and $K_{\rm s}$ filters.[6] With respect to metallicity, the difference between, e.g. solar and half-solar metallicity isochrones for a given age is small, to within the 2MASS photometric uncertainties. Thus, for simplicity, we adopt the solar metallicity ones.

Although several analytical approaches for CMD fitting are available (see a summary in Naylor & Jeffries 2006), we employ a more direct comparison of the isochrones with the decontaminated CMD morphology. Specifically, the fits are made *by eye*, using the combined main sequence (MS) and evolved stellar distributions as constraint. We also take variations due to photometric uncertainties into account (which, because of the restrictions imposed in Section 3, are usually small) and the presence of binaries (which tend to produce a redwards bias in the MS). Starting with the isochrones set for zero distance modulus and reddening, we shift them in magnitude and colour until a satisfactory match[7] with the CMD is obtained. The *best fits*, according to this approach, are shown in Figs 3–5

[6] http://stev.oapd.inaf.it/cgi-bin/cmd. These isochrones are very similar to the Johnson–Kron–Cousins ones (e.g. Bessel & Brett 1988), with differences of at most 0.01 mag in colour (Bonatto, Bica & Girardi 2004).

[7] Any isochrone solution that occurs within the photometric error bars is taken as acceptable.

Downloaded from http://mnras.oxfordjournals.org/ at FundaÃ§Ã£o Coordenação de Aperfeiçoamento de Pessoal de NÃ-vel Superior on February 24, 2014

Table 1. Fundamental parameters.

			WEBDA							This work				
Cluster	α(2000)	δ(2000)	Age	$E(B-V)$	$d_\odot$	D	α(2000)	δ(2000)	ℓ	b	Age	$E(B-V)$	$d_\odot$	ΔR_{SC}
	(hms)	(° ′ ″)	(Myr)	(mag)	(kpc)	(arcmin)	(hms)	(° ′ ″)	(°)	(°)	(Myr)	(mag)	(kpc)	(kpc)
(1)	(2)	(3)	(4)	(5)	(6)	(7)	(8)	(9)	(10)	(11)	(12)	(13)	(14)	(15)
Ru 1	06:36:25	−14:10:48	580	0.15	1.1	5.0	06:36:21.63	−14:08:48.75	223.95	−9.68	500 ± 100	0.26 ± 0.06	1.72 ± 0.16	1.31 ± 0.12
Ru 10	07:06:25	−20:05:00	–	–	–	4.0	07:06:29.05	−20:06:31.50	232.55	−5.85	500 ± 100	0.64 ± 0.06	2.34 ± 0.22	1.62 ± 0.14
Ru 23	07:30:41	−23:23:00	–	–	–	4.0	07:30:38.80	−23:23:36.00	238.08	−2.40	600 ± 100	0.54 ± 0.06	3.06 ± 0.29	2.00 ± 0.16
Ru 26	07:37:11	−15:38:59	30	0.10	1.4	24.0	07:37:11.10	−15:39:46.50	232.06	+2.68	400 ± 50	0.35 ± 0.06	1.82 ± 0.17	1.24 ± 0.11
Ru 27	07:37:30	−26:31:42	250	0.15	0.6	21.6	07:37:40.89	−26:31:45.50	241.60	−2.53	900 ± 100	0.03 ± 0.06	1.49 ± 0.14	0.82 ± 0.07
Ru 34	07:45:55	−20:23:00	–	–	–	6.0	07:45:56.22	−20:23:24.00	237.20	+2.16	1000 ± 100	0.00 ± 0.06	2.63 ± 0.25	1.70 ± 0.14
Ru 35	07:46:13	−31:17:00	–	–	–	1.5	07:46:13.64	−31:16:47.25	246.66	−3.25	400 ± 100	0.45 ± 0.10	3.91 ± 0.56	2.26 ± 0.28
Ru 37	07:49:54	−17:17:00	–	–	–	4.0	07:49:47.53	−17:14:46.50	234.94	+4.53	3000 ± 1000	0.00 ± 0.06	5.25 ± 0.74	3.87 ± 0.45
Ru 41	07:53:49	−26:58:00	–	–	–	2.0	07:53:48.38	−26:57:39.00	243.78	+0.37	700 ± 100	0.13 ± 0.10	3.15 ± 0.45	1.84 ± 0.23
Ru 54	08:11:21	−31:57:00	–	–	–	3.0	08:11:20.92	−31:56:49.50	250.03	+0.96	800 ± 100	0.13 ± 0.10	5.47 ± 0.78	3.22 ± 0.43
Ru 60	08:24:27	−47:13:00	–	–	–	3.0	08:24:26.29	−47:12:51.01	264.10	−5.51	400 ± 100	0.64 ± 0.10	6.16 ± 0.88	2.74 ± 0.54
Ru 63	08:32:40	−48:18:00	–	–	–	3.0	08:32:39.60	−48:18:19.50	265.80	−5.02	500 ± 100	0.61 ± 0.10	3.76 ± 0.37	1.16 ± 0.17
Ru 66	08:40:33	−38:04:00	–	–	–	2.0	08:40:33.82	−38:04:47.99	258.49	+2.28	600 ± 100	0.90 ± 0.10	3.76 ± 0.54	1.56 ± 0.24
Ru 152	07:54:30	−38:14:00	–	–	–	3.0	07:54:28.35	−38:14:14.26	253.54	−5.30	600 ± 100	0.67 ± 0.10	8.02 ± 1.15	5.00 ± 0.73
Ru 174	20:43:30	+37:03:00	–	–	–	8.0	20:43:30.48	+37:01:26.26	78.02	−3.39	800 ± 100	0.32 ± 0.06	2.11 ± 0.20	−0.13 ± 0.07

Note. Column 7: diameter estimated from optical images (Dias et al. 2002); Column 14: distance from the Sun; Column 15: distance from the solar circle.

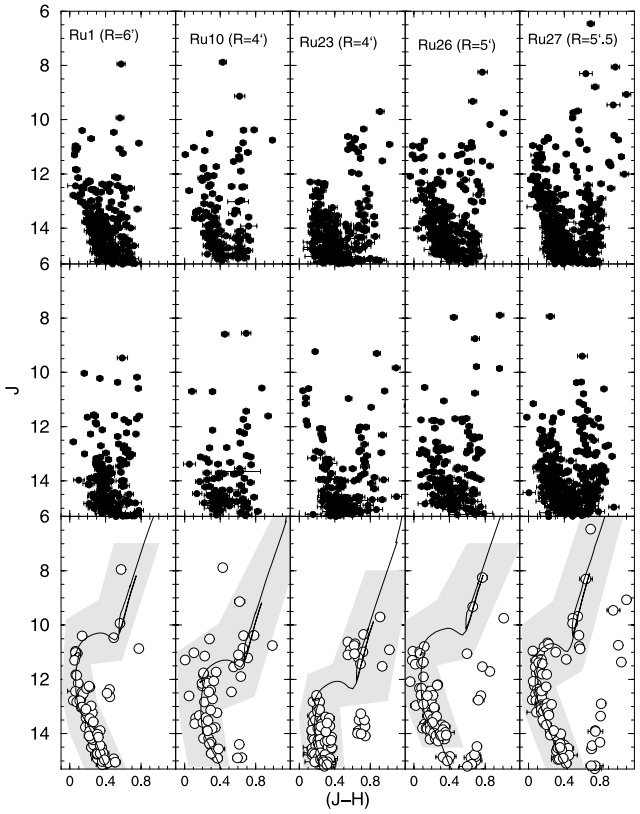

Figure 3. $J \times (J - H)$ CMDs of Ru 1, 10, 23, 26 and 27, showing the observed photometry for representative regions (top panels) and the equal-area comparison fields (middle). The decontaminated CMDs are shown in the bottom panels, together with the isochrone solution (solid line) and colour–magnitude filter (shaded polygon). Note that, for most stars, the error bars are smaller than the symbol.

(bottom panels), and the respective fundamental parameters are given in Table 1.

We derive ages within 400 Myr–1 Gyr, except for Ru 37, which seems to be somewhat older, with an age of ∼3 Gyr. As expected of optical clusters, the reddening values are relatively low, $E(B - V) \leq 0.9$ (or $A_V \leq 2.8$). In general, they are distant from the Sun [$1.5 \leq d_\odot(\mathrm{kpc}) \leq 8.0$], and located outside the solar circle [$0.8 \leq \Delta R_{SC}(\mathrm{kpc}) \leq 5.0$], except for Ru 174 at $\Delta R_{SC} \sim -0.13$ kpc.

Our sample has three clusters in common with Kharchenko et al. (2005). Within the uncertainties, both works agree on the age of Ru 1 (500–600 Myr); however, we find values of reddening and distance from the Sun about 60 per cent higher. For Ru 26 and Ru 27, they find ages significantly younger than this paper, especially for Ru 27 with 30 Myr as compared to 400 Myr. Reddening and distance from the Sun also present significant discrepancies (Table 1). A probable source for such differences is the presence of unaccounted for field stars in the analysis of Kharchenko et al. (2005). As can be seen in the decontaminated CMDs of Ru 1, Ru 26 and Ru 27 (Fig. 3), the age (and consequently the reddening and distance) is quite constrained, to within the quoted errors in Table 1. Similar reasons may also explain the differences we find with respect to the parameters derived by Vázquez et al. (2008) for Ru 10 [$E(B - V) = 0.25 \pm 0.15$, $d_\odot = 2.5 \pm 0.4$, kpc, and age = 800 ± 150 Myr], and Moitinho et al. (2006) for Ru 35 ($d_\odot \sim 5.32$, kpc, and age ∼70 Myr).

Downloaded from http://mnras.oxfordjournals.org/ at FundaÃ§Ã£o CoordenaÃ§Ã£o de AperfeiÃ§oamento de Pessoal de NÃ-vel Superior on February 24, 2014

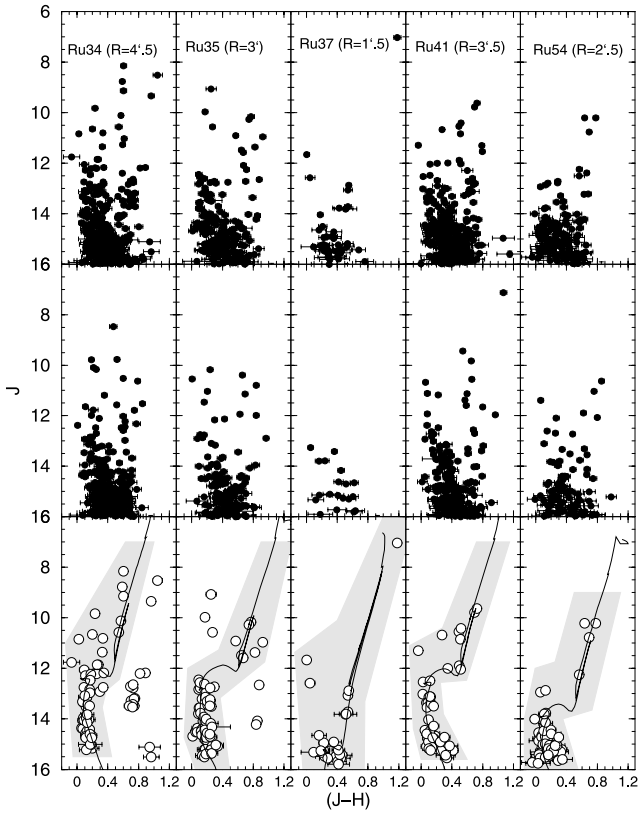

Figure 4. Same as Fig. 3 for Ru 34, 35, 37, 41 and 54.

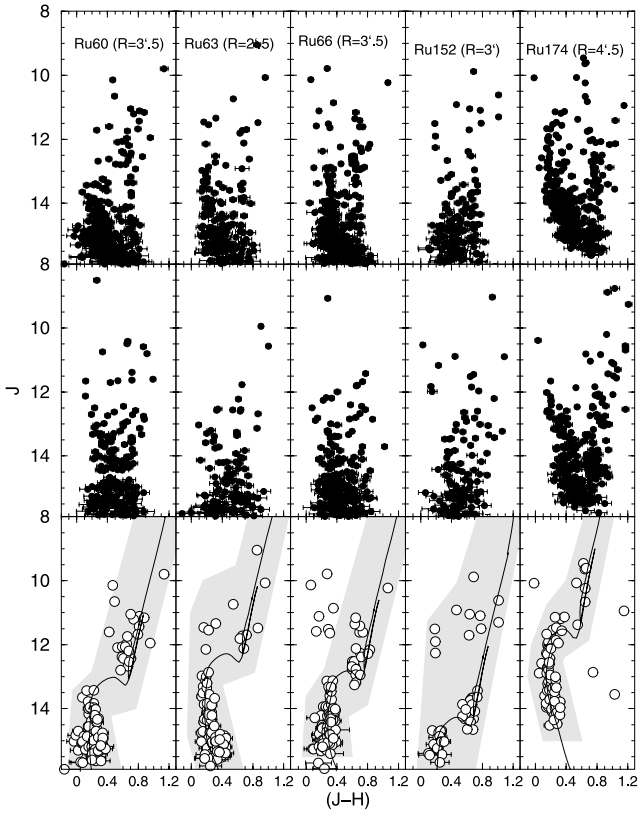

Figure 5. Same as Fig. 3 for Ru 60, 63, 66, 152 and 174.

5 STRUCTURAL PARAMETERS

Based on the decontaminated CMD morphologies and corresponding isochrone solutions (Figs 3–5), we build a colour–magnitude filter for each cluster. By excluding stars with colours not compatible with those of the cluster,[8] noise in the RDPs is minimized, while the contrast with the background is enhanced (e.g. Bonatto & Bica 2007b).

To preserve spatial resolution along the full radial range and, at the same time keeping moderate error bars, the RDPs are built in rings of increasing width with distance from the cluster centre. The set of ring widths used is $\Delta R = 0.25$, 0.5, 1.0, 2.5 and 5 arcmin, respectively for $0 \leq R < 0.5$, $0.5 \leq R < 2$, $2 \leq R < 5$, $5 \leq R < 20$ and $R \geq 20$ arcmin. Obviously, for any magnitude range, field stars with the same colour as the cluster's will not be excluded by the above filtering process. This gives rise to a residual background level, which can be measured as the average number density of stars away from the cluster. The R coordinate (and uncertainty) of each ring corresponds to the average position (and standard deviation) of the stars inside the ring. The resulting RDPs (and residual background) are shown in Fig. 7. Note that Ru 152 is located at ≈30 arcmin to the north-west of NGC 2477, which causes a conspicuous bump in the RDP.

We also estimate the cluster radius ($R_{\rm RDP}$) by measuring the distance from the centre where the cluster RDP and residual background are statistically indistinguishable. In this sense, $R_{\rm RDP}$ can be considered as an observational truncation radius, whose value depends both on the radial distribution of member stars and the field density.

[8] Note that the colour–magnitude filters are wide enough to take photometric uncertainties and binaries into account (or other multiple systems).

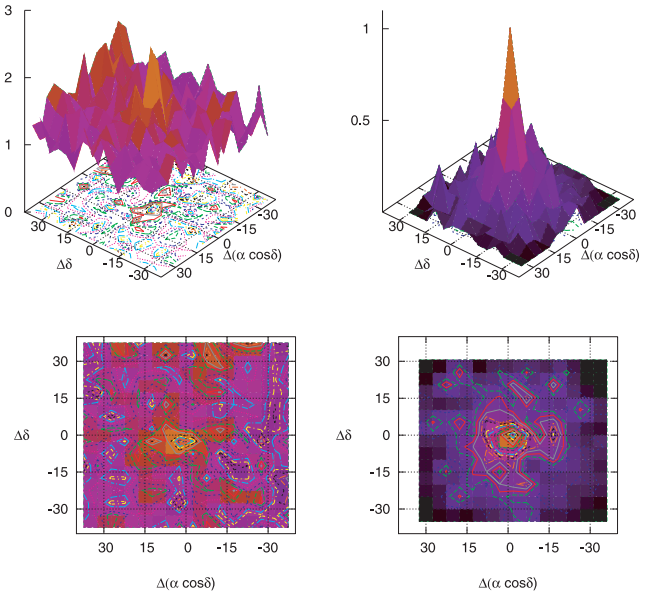

Figure 6. 2D perspective on Ru 1's field decontamination. Top panel: stellar surface density σ(stars arcmin^{-2}) computed before (left-hand panel) and after (right-hand panel) decontamination. Bottom panel: the respective isopleths. $\Delta[\alpha\ \cos(\delta)]$ and $\Delta\delta$ in arcmin.

The above RDPs are fitted with the function $\sigma(R) = \sigma_{\rm bg} + \sigma_0/[1 + (R/R_{\rm c})^2]$, where σ_0 and $\sigma_{\rm bg}$ are the central and residual background stellar densities, and $R_{\rm c}$ is the core radius. When applied to star counts, this function is similar to that used by King (1962) to the surface-brightness profiles in the central parts of globular clusters. Degrees of freedom are minimized by allowing only

Downloaded from http://mnras.oxfordjournals.org/ at FundaÃ§Ã£o CoordenaÃ§Ã£o de AperfeiÃ§oamento de Pessoal de NÃ-vel Superior on February 24, 2014

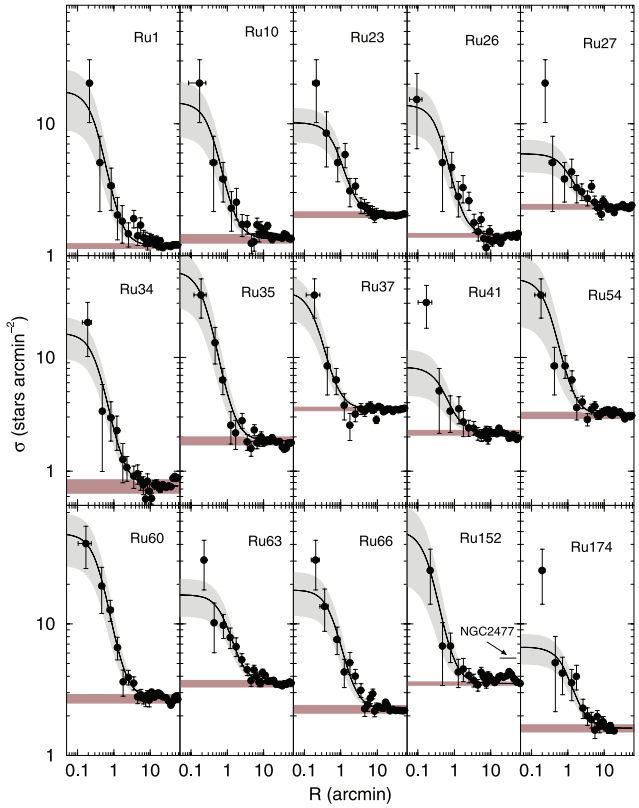

Figure 7. Stellar RDPs (filled circles) together with the best-fitting King-like profile (solid line), the 1σ uncertainty (light-shaded region) and the residual background level (shaded polygon). Note the pronounced central cusps in Ru 23, 27, 41, 63 and 174. The excess in the RDP of Ru 152 at $R \approx 20$–40 arcmin is due to NGC 2477.

σ_0 and R_c to vary in the fits, while σ_{bg} is previously measured in the surrounding field and kept fixed. The best-fitting solutions are shown in Fig. 7, and the corresponding structural parameters are given in Table 2.

Within uncertainties, the adopted King-like function provides a reasonable description along the full radial range of the RDPs for most of the sample (Fig. 7). The exceptions are Ru 27, Ru 41 and Ru 174, which present a pronounced cusp (density excess over the King-like fit) in the innermost RDP bin. The same appears to apply to Ru 23 and Ru 63, although only at the 1σ level. This feature has been attributed to a post-core collapse structure in some globular clusters (e.g. Trager, King & Djorgovski 1995). However, such a dynamical evolution-related feature has also been detected in the RDP of some Gyr-old OCs, e.g. NGC 3960 (Bonatto & Bica 2006) and LK 10 (Bonatto & Bica 2009). Alternatively, clusters that form dynamically cool and with significant substructure will probably develop an irregular central region, unless such a region collapses and smooths-out the initial substructure (Allison et al. 2009).

Compared to the distribution of core radii derived for a sample of relatively nearby OCs by Piskunov et al. (2007) – their fig. 3, the present clusters occupy the small-R_c tail. However, we find significant differences, especially in R_c, for the three clusters in common with Kharchenko et al. (2005). While they find angular values of R_{RDP} about twice those we derive, their angular values of R_c are ≈5 (Ru 27) and ≈15 (Ru 1 and Ru 26) times larger. This, in turn, would imply core radii of the order of ∼2.5 to ∼4.0 pc, bigger than most of the Galactic globular clusters (see e.g. fig. 8 of Bonatto & Bica 2008b). These discrepancies probably arise from the fact that they do not field-decontaminate their photometry. Because of the low-contrast RDPs that result when field stars are not eliminated, structural radii derived from RDP fits may not be robust.

Finally, according to Bonatto & Bica (2008a), the depth-limited 2MASS photometry has only a small effect on the core radius determination (by means of the King-like fit), but may be somewhat more important for R_{RDP}, especially in Ru 37, for which stars fainter than the main-sequence turnoff (MSTO) are not detected.

6 DISCUSSION

In the previous sections we derived a set of fundamental and structural parameters for a sample of 15 overlooked Ruprecht clusters. Now we use these parameters for comparison with the previously analysed Ruprecht clusters listed in WEBDA, as well as to investigate relations among parameters.

Table 2. Structural parameters derived from the RDPs.

Cluster	σ_0 (stars arcmin^{-2})	R_c (arcmin)	R_{RDP} (arcmin)	1 arcmin (pc)	σ_0 (stars pc^{-2})	R_c (pc)	R_{RDP} (pc)
(1)	(2)	(3)	(4)	(5)	(6)	(7)	(8)
Ru1	16.5 ± 8.4	0.32 ± 0.10	8.0 ± 1.0	0.499	66.1 ± 33.8	0.16 ± 0.05	4.0 ± 1.0
Ru10	13.1 ± 6.4	0.39 ± 0.12	4.0 ± 0.5	0.679	28.4 ± 13.9	0.26 ± 0.08	2.7 ± 0.3
Ru23	8.2 ± 2.9	0.79 ± 0.20	6.0 ± 0.5	0.888	10.3 ± 3.7	0.70 ± 0.18	5.3 ± 0.4
Ru26	12.5 ± 5.4	0.42 ± 0.13	5.5 ± 0.5	0.527	45.0 ± 19.4	0.22 ± 0.07	2.9 ± 0.3
Ru27	3.6 ± 1.6	1.05 ± 0.37	5.5 ± 0.5	0.433	19.0 ± 8.5	0.45 ± 0.16	2.4 ± 0.2
Ru34	15.6 ± 6.4	0.34 ± 0.08	4.5 ± 0.5	0.763	26.8 ± 11.0	0.26 ± 0.06	3.4 ± 0.4
Ru35	55.3 ± 28.8	0.24 ± 0.08	3.0 ± 0.5	1.135	42.9 ± 22.3	0.27 ± 0.09	3.4 ± 0.6
Ru37	34.1 ± 15.0	0.20 ± 0.06	1.4 ± 0.2	1.522	14.7 ± 6.5	0.30 ± 0.09	2.1 ± 0.3
Ru41	6.0 ± 3.5	0.47 ± 0.20	3.5 ± 0.5	0.913	7.2 ± 4.2	0.43 ± 0.18	3.2 ± 0.5
Ru54	45.9 ± 29.9	0.29 ± 0.15	3.0 ± 0.5	1.586	18.3 ± 11.9	0.46 ± 0.24	4.7 ± 0.8
Ru60	45.5 ± 20.4	0.39 ± 0.11	4.0 ± 0.5	1.786	14.3 ± 6.4	0.70 ± 0.20	7.1 ± 0.9
Ru63	13.1 ± 5.2	0.90 ± 0.25	7.0 ± 1.0	1.090	11.0 ± 4.3	0.98 ± 0.27	7.6 ± 1.1
Ru66	15.9 ± 6.5	0.64 ± 0.18	4.0 ± 0.5	1.091	6.2 ± 2.5	0.99 ± 0.29	6.4 ± 0.8
Ru152	47.0 ± 32.0	0.20 ± 0.08	3.5 ± 0.5	2.325	8.7 ± 5.6	0.47 ± 0.19	8.1 ± 1.2
Ru174	5.0 ± 1.7	0.94 ± 0.24	4.8 ± 0.5	0.613	13.4 ± 0.5	0.58 ± 0.15	2.9 ± 0.3

Note. Column 6: arcmin to parsec scale. For comparison with other clusters, the King-like central stellar density (σ_0) and core radius (R_c), together with the cluster radius (R_{RDP}), are given both in angular and in absolute units.

Downloaded from http://mnras.oxfordjournals.org/ at FundaÃ§Ã£o Coordenação de Aperfeiçoamento de Pessoal de NÃ-vel Superior on February 24, 2014

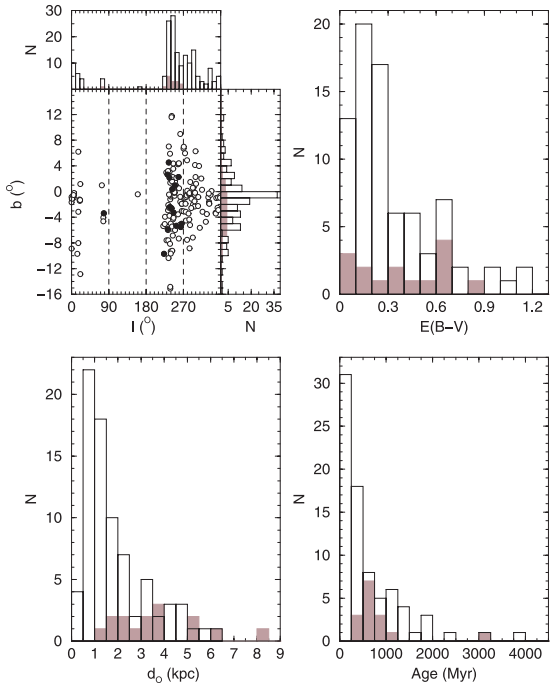

Figure 8. General properties of the present OCs (filled circles and shaded histograms) compared to the Ruprecht clusters (empty circles and histograms) listed in WEBDA. Dashed lines in the $\ell \times b$ diagram show the borders of the Galactic quadrants.

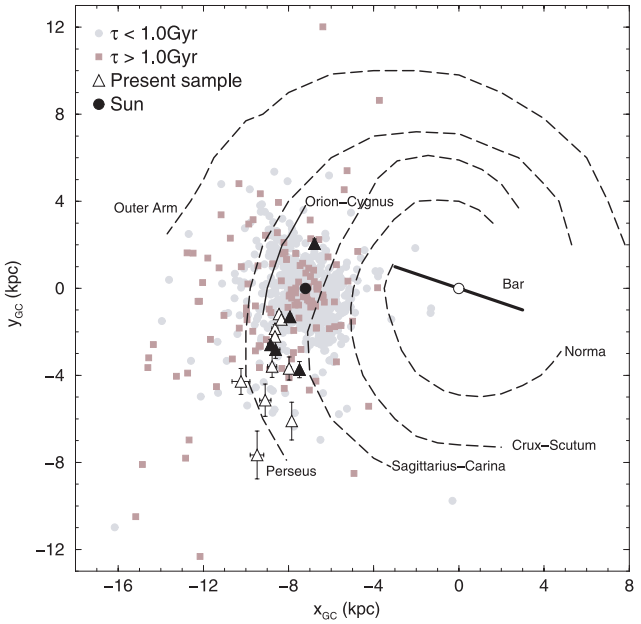

Figure 9. Schematic projection of the Galaxy, as seen from the North pole, with 7.2 kpc as the Sun's distance to the Galactic centre, in which the projected distribution of the present Ruprecht star clusters (triangles) is compared to the WEBDA OCs younger (circles) and older than 1 Gyr (squares). Clusters with the central cusp (Fig. 7) are shown as filled triangles. Main Galactic structures are identified.

6.1 Comparison with the Ruprecht OCs in WEBDA

WEBDA contains 171 such clusters with coordinates, but only 79 have age, reddening and distance from the Sun been determined so far.

The ℓ and b distribution of the Ruprecht clusters in WEBDA is shown in Fig. 8. By far, most of them are located in the third and fourth quadrants, and within $|b| \lesssim 8^\circ$. Our sample shares the same b distribution but is restricted essentially to the third quadrant. With respect to the age and reddening distributions, our sample basically maps those of the WEBDA clusters. However, our sample is biased towards larger values of the distance from the Sun, which is consistent with the fact that they still have not been studied in detail.

6.2 Location in the Galaxy

The positions of the sample clusters, projected on to the Galactic plane, are shown in Fig. 9, which contains the spiral arm structure of the Milky Way based on Momany et al. (2006) and Drimmel & Spergel (2001), derived from H II regions and molecular clouds (e.g. Russeil 2003). The Galactic bar is shown with an orientation of 14° and 6 kpc of total length (Freudenreich 1998; Vallée 2005). For comparison, we also include the OCs with age and distance from the Sun given in WEBDA, separated in two age groups, clusters younger or older than 1 Gyr.

The main features that emerge from Fig. 9 are summarized as follows. With respect to the Sun, all directions show a depletion in the number of detected OCs for distances farther than ∼2 kpc. This occurs because completeness effects (due to crowding and high background levels) together with enhanced disruption rates begin to affect critically regions more distant than ∼2 kpc, especially towards the bulge (e.g. Bonatto et al. 2006). Given the high dissolution rates in the inner Galaxy associated with dynamical interactions with the disc, the tidal pull of the bulge, and collisions with giant molecular clouds (e.g. Friel 1995; Bergond, Leon & Guilbert 2001; Bonatto & Bica 2007a), old OCs are found preferentially outside the solar circle, a region with relatively low tidal stress. On the other hand, the presence of bright stars in young OCs allows them to be detected farther than the old ones, especially towards the central Galaxy. It should be noted that WEBDA contains essentially optically selected OCs, and when surveys in the near-infrared are conducted – like the present one, an increasing number of (basically old) OCs at large distances from the Sun are being found. Near-infrared searches, in turn, might minimize the OC incompleteness around the Sun, but the problem for large distances would still remain (e.g. Bonatto et al. 2006).

Most of the present sample is located between the Perseus and Sagittarius-Carina arms, except for Ru 37 and especially Ru 152 that are beyond the Perseus arm. Given their age range (400 Myr–3 Gyr), it is quite possible that some of them may have suffered tidal stress from the arms, by means of encounters with giant molecular clouds. Collision with such clouds is another potential dissolution mechanism, especially for low-mass clusters (e.g. Wielen 1971, 1991; Gieles et al. 2006; Gieles, Athanassoula & Portegies Zwart 2007). Such events might have accelerated the dynamical evolution and produced changes in the cluster structure. However, we note that there is no difference in the projected positions of the clusters that display the central cusp in the RDP (Fig. 7) with respect to the King-like ones. In any case, it would be necessary to re-construct their orbits through the Galaxy for a deeper analysis on this issue.

6.3 Cluster size dependencies

Despite the considerable scatter, a first-order dependence of cluster size on Galactocentric distance is suggested in Fig. 10 (panel a).

© 2010 The Authors. Journal compilation © 2010 RAS, MNRAS **407,** 1728–1738

Downloaded from http://mnras.oxfordjournals.org/ at FundaÃ§Ã£o CoordenaÃ§Ã£o de AperfeiÃ§oamento de Pessoal de NÃ-vel Superior on February 24, 2014

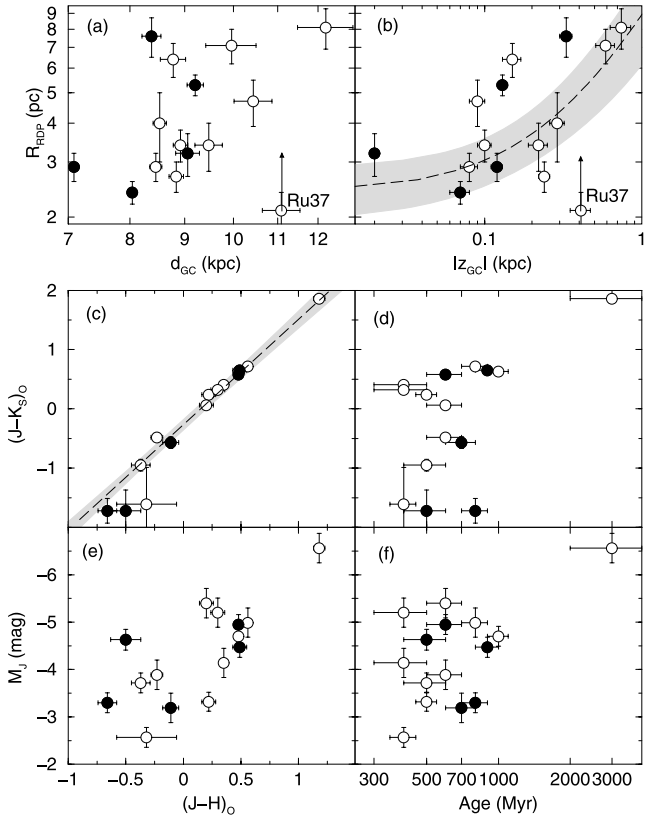

Figure 10. Top: relation of the cluster radius with Galactocentric distance (left) and distance from the plane (right). Arrows indicate the lower limit of $R_{\rm RDP}$ for Ru 37. Middle: dependence of the integrated $(J-K_{\rm s})_0$ colour on $(J-H)_0$ (left) and cluster age (right). Bottom: same as above for the absolute J magnitude. Clusters with the central cusp (Fig. 7) are shown as filled circles. Dashed line in (b): $R_{\rm RDP}({\rm pc}) = (2.4\pm0.4)+(6.5\pm2.7)\times|Z_{\rm GP}({\rm kpc})|$. Dashed line in (c): $(J-K_{\rm s})_0 = (-0.27\pm0.04)+(1.78\pm0.06)\times(J-H)_0$. Shaded region in (b) and (c): 1σ fit uncertainty.

Incidentally, the discordant cluster is Ru 37 ($R_{\rm RDP}\approx 2.1$ pc), the oldest one ($\sim$3 Gyr) of our sample. Given the age and distance from the Sun ($d_\odot\sim 5$ kpc) of Ru 37, stars fainter than the MSTO are not detected by 2MASS, which may have underestimated its size. Such a relation has already been observed (e.g. Lyngå 1982; van den Bergh, Morbey & Pazder 1991; Tadross et al. 2002), and may reflect the low dissolution rates associated with large Galactocentric distances. The rather weak correlation may be partly due to the fact that our sample clusters are located essentially outside the solar circle.

This point can be further investigated by examining the dependence of cluster size on the vertical distance to the Galactic plane $|Z_{\rm GP}|$, since our clusters are located within $|Z_{\rm GP}|\lesssim 1.0$ kpc. With the exception of Ru 37, a somewhat tight correlation shows up between $R_{\rm RDP}$ and $|Z_{\rm GP}|$. Indeed, excluding Ru 37, the remaining points are roughly described by the relation $R_{\rm RDP}({\rm pc}) = (2.4\pm0.4)+(6.5\pm2.7)\times|Z_{\rm GP}({\rm kpc})|$. Again, this relation is consistent with a lower-frequency of encounters with giant molecular clouds and the disc for OCs at high $|Z_{\rm GP}|$ with respect to those orbiting closer to the plane. However, we note that part of this effect may be related to completeness. Given that the average background+foreground contamination decreases with increasing $|Z_{\rm GP}|$, the external parts of an OC (where the surface brightness is intrinsically low) can be detected at larger distances for high-$|Z_{\rm GP}|$ objects than for those near the plane (Bonatto et al. 2006). On average, clusters at high $|Z_{\rm GP}|$ will tend to seem bigger than near the plane.

6.4 Integrated colours and magnitudes

Having decontaminated the photometry (Section 3) and derived structural parameters (Section 5), we now proceed to compute the integrated (apparent and absolute) magnitudes and reddening-corrected colours for the 2MASS bands. Since the decontamination efficiency is lower than 100 per cent (Section 3), we start by applying the colour–magnitude filter to the decontaminated photometry. Then we sum the flux (for a given band) of all stars within $R\leq R_{\rm RDP}$ (Table 2) to compute the cluster+residual field stars flux ($F_J^{\rm cl+fs}=\sum_i 10^{-0.4J_i}$). The same is done for all the comparison field stars, to estimate the residual contamination flux ($F_J^{\rm fs}$). Thus, the integrated magnitude is given by $m_J=-2.5\log\left(F_J^{\rm cl+fs}-\Omega\times F_J^{\rm fs}\right)$, where Ω is the ratio between the projected areas of the cluster and the comparison field. This procedure is applied to the J, H and $K_{\rm s}$ bands, and should minimize decontamination efficiency effects.

Since all clusters contain giant and MSTO stars (Figs 3–5) – which by far dominate the luminosity, the integrated magnitudes should not be significantly affected by the non-detection of the lower MS stars associated with the depth-limited 2MASS photometry. Reddening and distance from the Sun (for the absolute magnitude and reddening-corrected colours) are those computed in Section 4. The results are given in Table 3 and discussed below.

The integrated and reddening-corrected $(J-K_{\rm s})_0$ and $(J-H)_0$ colours are tightly related by $(J-K_{\rm s})_0=(-0.27\pm0.04)+(1.78\pm0.06)\times(J-H)_0$ (Fig. 10, panel c), and redder clusters also tend to be brighter in J (e). Panels (d) and (f) seem to show a slight tendency of old clusters to be redder and brighter than the young ones. This is consistent with most of the stellar luminosity (especially for the more massive stars) being transferred from the optical to the near-infrared, as star clusters become older. As a caveat, the latter relation hinges essentially on a single cluster with $\sim$3 Gyr of age. Thus, with the present data we cannot quantify the role of age in driving the near-infrared colours (panels c and d), since the age for most of the present OCs are restricted to the range 400 Myr $\sim$ 1 Gyr.

As far as we are aware, there is no study of OC integrated colours or magnitudes linking the near-infrared to the optical. However, if we assume that OCs and globular clusters follow similar scaling relations – at least with respect to integrated colours and magnitudes, we can use the Galactic globular clusters (MWGCs) both for comparison and to search for such a link. For this purpose, we use the integrated and reddening-corrected $(V-K_{\rm s})_0$, $(J-H)_0$ and $(J-K_{\rm s})_0$ colours computed for a large set of MWGCs on 2MASS images (Cohen et al. 2007), coupled to the respective absolute M_V magnitudes from Harris (1996, together with the 2003 revision). The results are summarized in Fig. 11 (top panels). Consistent with their old ages, the MWGCs $(J-K_{\rm s})_0$ and $(J-H)_0$ colours (panel a) are restricted to a narrow range (the spread is essentially due to the different metallicities and partly to unaccounted for reddening), when compared to the set of (younger) Ruprecht OCs (Fig. 10, panel c). Besides, the near-IR MWGC colours follow a similar – although somewhat flatter [$(J-K_{\rm s})_0\propto 1.2\times(J-H)_0$] – relation than our Ruprecht OCs [$(J-K_{\rm s})_0\propto 1.8\times(J-H)_0$]. Finally, with respect to the absolute magnitudes M_V and M_J (panel b), the MWGCs are tightly related by $M_V=(1.41\pm0.27)+(0.96\pm0.03)\times M_J$, over the relatively wide ranges $-12\lesssim M_V\lesssim -6.5$ and $-10\lesssim M_J\lesssim -4.5$. Note that the few discordant points can be accounted for by a reddening under-correction.

Downloaded from http://mnras.oxfordjournals.org/ at FundaÃ§Ã£o Coordenação de Aperfeiçoamento de Pessoal de NÃ-vel Superior on February 24, 2014

Table 3. Integrated magnitude and colours.

	Apparent				Absolute/reddening corrected					
Cluster	m_J	$(J-H)$	$(J-K_s)$	$(H-K_s)$	m_J	M_V	$(J-H)_0$	$(J-K_s)_0$	$(H-K_s)_0$	$(V-J)_0$
(1)	(2)	(3)	(4)	(5)	(6)	(7)	(8)	(9)	(10)	(11)
Ru 1	8.08 ± 0.03	$+0.30 \pm 0.06$	$+0.37 \pm 0.06$	$+0.06 \pm 0.08$	-3.3 ± 0.2	-1.8 ± 0.3	$+0.22 \pm 0.06$	$+0.24 \pm 0.06$	$+0.02 \pm 0.08$	1.5 ± 0.4
Ru 10	8.67 ± 0.02	-0.17 ± 0.08	-0.64 ± 0.10	-0.47 ± 0.13	-3.7 ± 0.2	-2.2 ± 0.4	-0.37 ± 0.08	-0.95 ± 0.10	-0.58 ± 0.13	1.6 ± 0.4
Ru 23	7.94 ± 0.01	$+0.65 \pm 0.03$	$+0.84 \pm 0.02$	$+0.19 \pm 0.03$	-4.9 ± 0.2	-3.3 ± 0.4	$+0.48 \pm 0.03$	$+0.58 \pm 0.02$	$+0.09 \pm 0.03$	1.6 ± 0.4
Ru 26	9.03 ± 0.06	-0.21 ± 0.26	-1.44 ± 0.62	-1.23 ± 0.67	-2.6 ± 0.2	-1.1 ± 0.3	-0.32 ± 0.26	-1.61 ± 0.62	-1.29 ± 0.67	1.5 ± 0.4
Ru 27	6.42 ± 0.03	$+0.49 \pm 0.06$	$+0.67 \pm 0.07$	$+0.17 \pm 0.08$	-4.5 ± 0.2	-2.9 ± 0.4	$+0.49 \pm 0.06$	$+0.65 \pm 0.07$	$+0.17 \pm 0.08$	1.6 ± 0.4
Ru 34	7.40 ± 0.01	$+0.48 \pm 0.03$	$+0.63 \pm 0.02$	$+0.15 \pm 0.03$	-4.7 ± 0.2	-3.1 ± 0.4	$+0.48 \pm 0.03$	$+0.63 \pm 0.02$	$+0.15 \pm 0.03$	1.6 ± 0.4
Ru 35	9.20 ± 0.02	$+0.49 \pm 0.03$	$+0.63 \pm 0.03$	$+0.14 \pm 0.03$	-4.1 ± 0.3	-2.6 ± 0.4	$+0.35 \pm 0.03$	$+0.41 \pm 0.03$	$+0.05 \pm 0.03$	1.6 ± 0.5
Ru 37	7.04 ± 0.02	$+1.18 \pm 0.05$	$+1.86 \pm 0.03$	$+0.68 \pm 0.05$	-6.6 ± 0.3	-4.9 ± 0.5	$+1.18 \pm 0.05$	$+1.86 \pm 0.03$	$+0.68 \pm 0.05$	1.7 ± 0.5
Ru 41	9.41 ± 0.03	-0.07 ± 0.07	-0.51 ± 0.10	-0.43 ± 0.11	-3.2 ± 0.3	-1.6 ± 0.4	-0.11 ± 0.07	-0.57 ± 0.10	-0.46 ± 0.11	1.5 ± 0.5
Ru 54	8.81 ± 0.02	$+0.60 \pm 0.02$	$+0.78 \pm 0.02$	$+0.18 \pm 0.02$	-5.0 ± 0.3	-3.4 ± 0.4	$+0.56 \pm 0.02$	$+0.72 \pm 0.02$	$+0.16 \pm 0.02$	1.6 ± 0.5
Ru 60	9.29 ± 0.03	$+0.50 \pm 0.06$	$+0.63 \pm 0.06$	$+0.14 \pm 0.08$	-5.2 ± 0.3	-3.6 ± 0.4	$+0.30 \pm 0.06$	$+0.32 \pm 0.06$	$+0.02 \pm 0.08$	1.6 ± 0.5
Ru 63	8.76 ± 0.03	-0.31 ± 0.13	-1.42 ± 0.35	-1.11 ± 0.37	-4.6 ± 0.2	-3.0 ± 0.4	-0.50 ± 0.13	-1.72 ± 0.35	-1.22 ± 0.37	1.6 ± 0.4
Ru 66	9.76 ± 0.02	$+0.05 \pm 0.05$	-0.04 ± 0.07	-0.09 ± 0.08	-3.9 ± 0.3	-2.3 ± 0.4	-0.23 ± 0.05	-0.48 ± 0.07	-0.26 ± 0.08	1.6 ± 0.5
Ru 152	9.69 ± 0.03	$+0.41 \pm 0.06$	$+0.39 \pm 0.06$	-0.01 ± 0.07	-5.4 ± 0.3	-3.8 ± 0.4	$+0.20 \pm 0.06$	$+0.06 \pm 0.06$	-0.13 ± 0.07	1.6 ± 0.5
Ru 174	8.60 ± 0.03	-0.56 ± 0.08	-1.56 ± 0.21	-1.00 ± 0.22	-3.3 ± 0.2	-1.8 ± 0.3	-0.66 ± 0.08	-1.72 ± 0.21	-1.05 ± 0.22	1.5 ± 0.4

Note. Magnitude and colours have been computed with the decontaminated photometry for the region $R \leq R_{\rm RDP}$ (Table 2). Reddening and distance from the Sun (for the absolute magnitude and reddening-corrected colours – Columns 6–9) are derived in Section 4. Columns 7 and 11: estimated M_V and $(V-J)_0$ (Section 6.4).

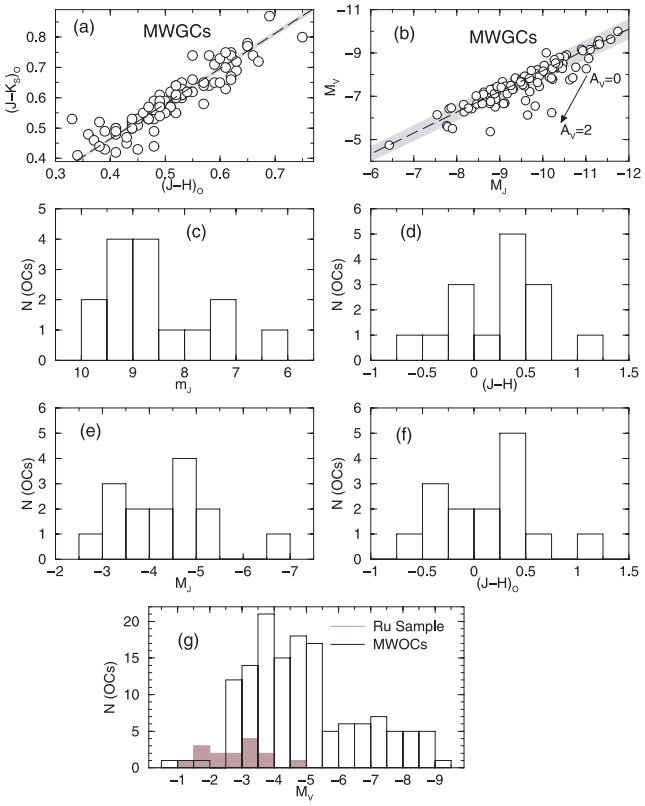

Figure 11. Panels (a) and (b): relations derived from MWGCs for the $(J-K_s)_0$ and $(J-H)_0$ colours $[(J-K_s)_0 = (1.16 \pm 0.01) \times (J-H)_0]$, and the absolute V and J magnitudes $[M_V = (1.41 \pm 0.27) + (0.96 \pm 0.03) \times M_J]$. Arrow in (b): reddening vector for $A_V = 2$. Panels (c) and (d): histograms for the number of OCs within bins of apparent J magnitude and $(J-H)$ colour. Panels (e) and (f): same as above for the absolute J magnitude and the reddening-corrected $(J-H)_0$ colour. Panel (g): the distribution of the extrapolated M_V values of our Ruprecht sample (shaded histogram) compared (empty histogram) to the Galactic OCs of Lata et al. (2002) and Battinelli et al. (1994).

The apparent J magnitude distribution of our sample clusters is clearly biased towards fainter objects (panel c of Fig. 11), with about half of the sample having $m_J \gtrsim 8.5$, while the absolute J magnitude (e) is roughly uniformly distributed around $\overline{M_J} \approx -4.5$, with a ± 2.0 mag spread. The observed (d) and reddening-corrected (f) $(J-H)$ colours are roughly distributed around the average value $\overline{(J-H)} \approx 0.5$, with a ± 1.0 mag spread.

Now, extrapolating the MWGC $M_V \times M_J$ relation to the M_J values derived for our Ruprecht clusters, we find M_V values in the range $-5 \lesssim M_V \lesssim -1$ (panel g of Fig. 11 and Table 3). Note that the integrated colour $(V-J)$ is similar in all cases, with an average value $\overline{(V-J)_0} = 1.6 \pm 0.5$. We now compare the Ruprecht M_V values with those measured for 140 Galactic OCs (MWOCs) by Lata et al. (2002) together with 106 OCs of Battinelli, Brandimarti & Capuzzo-Dolcetta (1994).[9] Most (≈72 per cent) of the MWOCs have M_V within $-5.5 \lesssim M_V \lesssim -2.5$, but the remaining ones can be as luminous as $M_V \approx -10$. Clearly, our Ruprecht clusters, in general, appear to be intrinsically faint in the optical, with an M_V distribution similar to – but still somewhat biased to lower luminosities than – the MWOCs.

7 SUMMARY AND CONCLUSIONS

Given the rather efficient and numerous dissolution mechanisms operating in the Galaxy, the majority of the OCs do not survive beyond a few 10^8 yr. In this context, it is important to investigate the structural and photometric properties of OCs that are undergoing this evolved phase.

This paper focuses on 15 overlooked Ruprecht clusters, 12 of them never before studied. With the exception of a single object at $\ell \approx 78^\circ$, the remaining clusters are located in the third Galactic quadrant, which minimizes the field-star contamination. We work with 2MASS photometry (with errors $\lesssim 0.15$ mag), on which we apply field-star decontamination to enhance CMD evolutionary

[9] Both samples have similar M_V distributions. For the OCs in common we have used the more recent values of Lata et al. (2002).

© 2010 The Authors. Journal compilation © 2010 RAS, MNRAS **407,** 1728–1738

Downloaded from http://mnras.oxfordjournals.org/ at FundaÃ§Ã£o CoordenaÃ§Ã£o de Aperfeiçoamento de Pessoal de NÃ-vel Superior on February 24, 2014

sequences and stellar RDPs, thus yielding more constrained fundamental and structural parameters.

As typical optically discovered clusters, the reddening values are relatively low, within $0.0 \lesssim E(B-V) \lesssim 0.9$; on the other hand, they are distant from the Sun, within $1.5 \lesssim d_{\odot}(\mathrm{kpc}) \lesssim 8.0$. The integrated apparent J magnitudes are rather faint, within $6.4 \lesssim m_J \lesssim 9.8$, but given the distances, the absolute magnitudes are relatively bright $-6.6 \lesssim M_J \lesssim -2.6$. The ages are in the range 400 Myr–1 Gyr, except for the significantly older Ru 37, with ∼3 Gyr. The RDPs are well contrasted with respect to the background and follow the King-like profile for most of the radial range. Exceptions are Ru 23, Ru 27, Ru 41, Ru 63 and Ru 174, which present a pronounced stellar density excess in the innermost RDP bin. The core radii of the present sample are small, when compared to those of nearby OCs (e.g. Piskunov et al. 2007). By extrapolating the relation between M_V and M_J, derived for globular clusters, we estimate $-5 \lesssim M_V \lesssim -1$, which suggests that they are low-luminosity optically selected clusters.

The sample clusters are located between (or close to) the Perseus and Sagittarius-Carina arms, and we present evidence that the cluster size increases both with Galactocentric distance and distance to the plane. The latter relation, in particular, is consistent with a low frequency of tidal stress associated with high-$|Z_{\mathrm{GP}}|$ regions.

It is clear from the above analysis that searches for star clusters in catalogues of candidates – even in the optical – are far from complete. Detailed investigations will certainly add more members to the present-day OC census. Besides, since young clusters are rather easy to identify even at large distances, the overlooked clusters are expected to be of the evolved/old age range. Thus, works like this one are important not only because reliable astrophysical parameters are derived for a sample of unstudied clusters. Perhaps the main importance lies in the unambiguous characterization of OCs with ages beyond several 10^8 yr. A better statistics on the population of these – and older – clusters can be used to investigate cluster formation rates and to constrain the time-scale of cluster dissolution in the Galaxy.

ACKNOWLEDGMENTS

We thank the reviewer, Dr A.F. Moffat, for interesting comments and suggestions. We acknowledge support from the Brazilian Institution CNPq. This publication makes use of data products from the Two Micron All Sky Survey, which is a joint project of the University of Massachusetts and the Infrared Processing and Analysis Centre/California Institute of Technology, funded by the National Aeronautics and Space Administration and the National Science Foundation. This research has made use of the WEBDA data base, operated at the Institute for Astronomy of the University of Vienna.

REFERENCES

Allison R. J., Goodwin S. P., Parker R. J., de Grijs R., Portegies Zwart S. F., Kouwenhoven M. B. N., 2009, ApJ, 700, L99
Alter G., Balázs B., Ruprecht J., Vanysek J., 1970, in Alter G., Balázs B., Ruprecht J., eds, Catalogue of Star Clusters and Associations, 2nd edn. Akademiai Kiado, Budapest
Battinelli P., Brandimarti A., Capuzzo-Dolcetta R., 1994, A&AS, 104, 379
Baumgardt H., Makino J., 2003, MNRAS, 340, 227
Bergond G., Leon S., Guilbert J., 2001, A&A, 377, 462
Bessel M. S., Brett J. M., 1988, PASP, 100, 1134
Bica E., Bonatto C., Camargo D., 2008, MNRAS, 385, 349
Bonatto C., Bica E., 2006, A&A, 455, 931
Bonatto C., Bica E., 2007a, A&A, 473, 445
Bonatto C., Bica E., 2007b, MNRAS, 377, 1301
Bonatto C., Bica E., 2008a, A&A, 477, 829
Bonatto C., Bica E., 2008b, A&A, 479, 741
Bonatto C., Bica E., 2009, MNRAS, 392, 483
Bonatto C., Bica E., 2010, A&A, in press (astro-ph/arXiv:1003.3611)
Bonatto C., Bica E., Girardi L., 2004, A&A, 415, 571
Bonatto C., Kerber L. O., Bica E., Santiago B. X., 2006, A&A, 446, 121
Cardelli J. A., Clayton G. C., Mathis J. S., 1989, ApJ, 345, 245
Carraro G., Janes K. A., Eastman J. D., 2005, MNRAS, 364, 179
Carraro G., Janes K. A., Costa E., Méndez R. A., 2006a, MNRAS, 368, 1078
Carraro G., Subramaniam A., Janes K. A., 2006b, MNRAS, 371, 1301
Cohen J. G., Hsieh S., Metchev S., Djorgovski S. G., Malkan M., 2007, AJ, 133, 99
Dias W. S., Alessi B. S., Moitinho A., Lépine J. R. D., 2002, A&A, 389, 871
Drimmel R., Spergel D. N., 2001, ApJ, 556, 181
Dutra C. M., Santiago B. X., Bica E., 2002, A&A, 383, 219
Freudenreich H. T., 1998, ApJ, 492, 495
Friel E. D., 1995, ARA&A 1995, 33, 381
Gieles M., Portegies Zwart S. F., Baumgardt H., Athanassoula E., Lamers H. J. G. L. M., Sipior M., Leenaarts J., 2006, MNRAS, 371, 793
Gieles M., Athanassoula E., Portegies Zwart S. F., 2007, MNRAS, 376, 809
Girardi L., Bertelli G., Bressan A., Chiosi C., Groenewegen M. A. T., Marigo P., Salasnich B., Weiss A., 2002, A&A, 391, 195
Goodwin S. P., Bastian N., 2006, MNRAS, 373, 752
Harris W. E., 1996, AJ, 112, 1487
Khalisi E., Amaro-Seoane P., Spurzem R., 2007, MNRAS, 374, 703
Kharchenko N. V., Piskunov A. E., Röser S., Schilbach E., Scholz R.-D., 2005, A&A, 438, 1163
King I., 1962, AJ, 67, 471
Lada C. J., Lada E. A., 2003, ARA&A, 41, 57
Lamers H. J. G. L. M., Gieles M., 2006, A&A, 455, L17
Lamers H. J. G. L. M., Gieles M., Bastian N., Baumgardt H., Kharchenko N. V., Portegies Zwart S., 2005, A&A, 441, 117
Lata S., Pandey A. K., Sagar R., Mohan V., 2002, A&A, 388, 158
Lyngå G., 1982, A&A, 109, 213
Moitinho A., Vázquez R. A., Carraro G., Baume G., Giorgi E. E., Lyra W., 2006, MNRAS, 368, L77
Momany Y., Zaggia S., Gilmore G., Piotto G., Carraro G., Bedin L. R., de Angeli F., 2006, A&A, 451, 515
Naylor T., Jeffries R. D., 2006, MNRAS, 373, 1251
Oort J. H., 1958, in O'Connell D. J. K., ed., Ricerche Astronomiche, Vol. 5, Specola Vaticana, Proc. Conf. at Vatican Observatory, Castel Gandolfo. North-Holland, Amsterdam, p. 415
Pavani D. N., Bica E., 2007, MNRAS, 468, 139
Piskunov A. E., Schilbach E., Kharchenko N. V., Röser S., Scholz R.-D., 2007, A&A, 468, 151
Russeil D., 2003, A&A, 397, 133
Skrutskie M. et al., 1997, in Garzon F., Burton B., Epchtein N., Omont A., Persi P., eds, The Impact of Large Scale Near-IR Sky Surveys, Vol. 210. Kluwer, Dordrecht, p. 187
Spitzer L., 1958, ApJ, 127, 17
Tadross A. L., Werner P., Osman A., Marie M., 2002, New Astron., 7, 553
Trager S. C., King I. R., Djorgovski S., 1995, AJ, 109, 218
Vallée J. P., 2005, AJ, 130, 56
van den Bergh S., Morbey C., Pazder J., 1991, ApJ, 375, 594
Vázquez R. A., May J., Carraro G., Bronfman L., Moitinho A., Baume G., 2008, ApJ, 672, 930
Wielen R., 1971, A&A, 13, 309
Wielen R., 1991, in Janes K., ed., ASP Conf. Ser. Vol. 13, The Formation and Evolution of Star Clusters. Astron. Soc. Pac., San Francisco, p. 343

This paper has been typeset from a TEX/LATEX file prepared by the author.

Downloaded from http://mnras.oxfordjournals.org/ at FundaÃ§Ã£o Coordenação de Aperfeiçoamento de Pessoal de NÃvel Superior on February 24, 2014